Published in final edited form as:
Biochemistry. 2013 March 19; 52(11): 1903–1912. doi:10.1021/bi400027y.

Resolution of Oligomeric Species during the Aggregation of $A\beta_{1-40}$ Using ^{19}F NMR

Yuta Suzuki[1], **Jeffrey R. Brender**[1,3], **Molly T. Soper**[1], **Janarthanan Krishnamoorthy**[1,3], **Yunlong Zhou**[4], **Brandon T. Ruotolo**[1], **Nicholas A. Kotov**[4], **Ayyalusamy Ramamoorthy**[1,3,*], and **E. Neil G. Marsh**[1,2,3,*]

[1]Department of Chemistry, University of Michigan, Ann Arbor, MI 48109

[2]Department of Biological Chemistry, University of Michigan, Ann Arbor, MI 48109

[3]Department of Biophysics, Chemical Engineering, Materials Science, University of Michigan, Ann Arbor, MI 48109

[4]Department of Biomedical Engineering, University of Michigan, Ann Arbor, MI 48109

Abstract

In the commonly used nucleation-dependent model of protein aggregation, aggregation proceeds only after a lag phase in which the concentration of energetically unfavorable nuclei reaches a critical value. The formation of oligomeric species prior to aggregation can be difficult to detect by current spectroscopic techniques. By using real-time ^{19}F NMR along with other techniques, we are able to show that multiple oligomeric species can be detected during the lag phase of $A\beta_{1-40}$ fiber formation, consistent with a complex mechanism of aggregation. At least 6 types of oligomers can be detected by ^{19}F NMR. These include the reversible formation of large β-sheet oligomer immediately after solubilization at high peptide concentration; a small oligomer that forms transiently during the early stages of the lag phase; and 4 spectroscopically distinct forms of oligomers with molecular weights between ~30–100 kDa that appear during the later stages of aggregation. The ability to resolve individual oligomers and track their formation in real-time should prove fruitful in understanding the aggregation of amyloidogenic proteins and in isolating potentially toxic non-amyloid oligomers.

The accumulation of misfolded proteins is a common pathological feature of a number of human disorders, including neurodegenerative disorders such as Alzheimer's and Parkinson's disease and several metabolic diseases such as type II diabetes. Under pathological conditions, the soluble precursor form of these proteins is triggered to self-assemble into amyloid fibers.(1) These are long, linear and often twisted structures a few nanometers in diameter and many nanometers in length.(2) The morphologies of amyloid fibers show a characteristic cross-β sheet X-ray diffraction pattern indicating a cross β-sheet conformation of β-sheets running perpendicular to the fibril axis.(2, 3)

In Alzheimer's disease, the amyloid plaques are largely composed of the Aβ peptide. Aβ peptides are derived from proteolytic of cleavage of the amyloid precursor protein (APP) to

*Corresponding authors: Dr. Neil Marsh, Department of Chemistry, University of Michigan, Ann Arbor MI 48109-1055, Tel 734 763 6096, FAX 734 615 3790, nmarsh@umich.edu. Dr. A. Ramamoorthy, Department of Chemistry, University of Michigan, Ann Arbor MI 48109-1055, Tel 734 764 1438, FAX 734 615 3790, ramamoor@umich.edu.

Supporting information
Additional figures illustrating DOSY NMR data, ^{19}F NMR spectra, peptide synthesis, AFM images acquired during the peptide aggregation, and ESI-MS spectra are available as supporting information. This material is available free of charge via the Internet at http://pubs.acs.org. The authors declare no competing financial interest.

produce peptides varying form 36–43 amino acids in length, of which $A\beta_{1-40}$ is the most common.(4) Because pathogenic mutations in the APP lead to early onset versions of Alzheimer's diseases and aggregated forms of $A\beta_{1-40}$ are toxic *in vivo,* and also to some extent in mouse models, Aβ plaque formation has been proposed to be the ultimate upstream cause of Alzheimer's disease (amyloid cascade hypothesis).(5–7) The process of amyloid formation has been repeatedly shown for multiple amyloidogenic proteins to disrupt the regular function of tissue. Unfortunately, how this occurs has been obscured by our lack of knowledge about the aggregation process itself.(4) In particular, identifying potentially toxic species in Aβ has been difficult because of the heterogeneity of the samples and inter-conversion among species.(8) NMR is attractive method for following the reaction in real-time because of the strong relationship between chemical shift and peptide structure. However, applications of real-time NMR to amyloid formation have been limited,(9, 10) largely due to spectral overlap 1D ^{1}H spectra and the difficulty of obtaining multidimensional spectra rapidly enough to follow aggregation.

^{19}F NMR is an attractive alternative because of the high sensitivity of the chemical shift of the ^{19}F nucleus to small changes in chemical environment; therefore it is possible to use simple 1D ^{19}F spectra to detect the changes of protein conformations.(11–17) In addition, fluorine is extremely rare in biological systems so that there is no competition from background signals, a problem that often afflicts measurements using ^{1}H, ^{13}C, and ^{15}N NMR.(18, 19) These advantages have been exploited to study large multi-protein complexes as well as to study proteins *in vivo*, where signals from protein of interest are often attenuated in other NMR techniques.(18)

Previously, we used ^{19}F NMR to study the oligomerization of IAPP, an amyloidogenic polypeptide implicated in β-cell death in type II diabetes.(20) These studies showed aggregation of IAPP to be essentially a two state event; monomeric IAPP is rapidly converted to fibrillar IAPP without the buildup of any intermediates small enough to be detected by ^{19}F NMR.(20) This finding is in agreement with other studies of IAPP aggregation, which show small oligomers of less than 100 kDa do not build up to an appreciable extent during aggregation.(21–23)

In contrast, many off- and on-pathway oligomeric intermediates of Aβ have been isolated, both *in vitro* and *in situ* from tissue samples of Alzheimer's patients. Characterization of these oligomeric species is particularly important as a current hypothesis holds that small to intermediate size (~5–6 nm in diameter) oligomers may be responsible for much of the toxicity of amyloid proteins.(24, 25) Furthermore, alternate mechanistic pathways can lead to alternate equilibrium structures (conformational polymorphism).(26) Conformational polymorphism is particularly important for the infectious amyloid particles known as prions in which it is believed to lead to transmission and cross-species barriers.(27) Here, we demonstrate ^{19}F NMR real-time measurements to investigate the formation of small oligomers during the formation of amyloid fibers from $A\beta_{1-40}$.

EXPERIMENTAL PROCEDURES

Synthesis of Fmoc-L-trifluoromethionine

The synthesis of Fmoc-L-homocysteine (Fmoc-hCys-Oh) was based on a modified version of the procedure of Jiang et al. (28) Bis-L-homocysteine was purchased from Toronto Research Chemicals Inc. A solution of Fmoc *N*-hydroxysuccinimide ester (Fmoc-Osu) in dioxane was added dropwise with vigorous stirring to L-homocysteine in 10% w/v $NaHCO_3$ (aq) overnight. After adjustment of the pH to 4 using citric acid, dioxane was removed under reduced pressure followed by extraction with ethyl acetate (3x). The ethyl acetate layers were combined, dried over anhydrous sodium sulfate, and evaporated under reduced

pressure to yield the pure product. It was then dissolved into a Dimethylformamide (DMF)/ H_2O solution followed by the addition of 1.5 eq. of tris(2-carboxyethyl)phosphine (TCEP), and the reaction mixture stirred overnight. DMF was then removed under reduced pressure and the aqueous solution was extracted with ethyl acetate (3x) to yield pure product. The overall yield for the two steps was 60 % without any purification step. The analytical data for Fmoc-hCys-Oh matched as previously reported data. (28, 29)

Fmoc-L-trifluoromethionine (Fmoc-tfMet-Oh) was then synthesized from Fmoc-hCys-Oh using the basic procedure developed by Togni and coworkers.(30) Togni reagent (1-Trifluoromethyl-3,3-dimethyl-1,2-benziodoxole) was purchased from TCI America. Briefly, a solution of Fmoc-L-homocysteine in methanol was cooled to −78 °C, and then 1 eq of Togni reagent was added dropwise with vigorous stirring. After completion of reaction overnight, the reaction mixture was dried under vacuum and purified by flash chromatography to yield desired product. The analytical data for Fmoc-tfMet-Oh matched the previously reported data.(31)

Peptide preparation

$A\beta_{1\text{-}40}$-tfMet35 peptide was synthesized manually by solid-phase Fmoc-based chemistry using the dimethoxybenzyl-protected (Dmb) dipeptide, Fmoc-Val-(Dmb)Gly-OH at positions 36 and 37 to disrupt aggregation during synthesis. Fmoc-tfMet-Oh was substituted for Met at position 35. The peptide was cleaved from the resin using 92.5 % TFA, 2.5 % H_2O, 2.5 % ethanedithiol, and 2.5 % anisole. The crude peptide was dissolved in 20 % acetic acid (v/v) and the purified by reverse-phase HPLC using a Waters semi-preparative C18 column equilibrated in 0.045% HCl. The peptides were eluted with a linear gradient of 0% to 80% acetonitrile at a flow rate of 10 ml/min. The identity of the purified peptide was confirmed using matrix-assisted laser desorption ionization mass spectroscopy, which gave corresponding to the correct mass of 4384.

Sample Preparation

To remove preformed aggregates, the purified peptide was dissolved in 2 % ammonium hydroxide followed by the removal of the solvent by lyophilization. The lyophilized peptide was first dissolved in 1 mM NaOH and sonicated for 15 min. The peptide solution was then buffered in 20 mM sodium phosphate (pH 7.4) and 10% D_2O and diluted to the desired peptide concentration. The sample solution was filtered though a 0.22 μm filter immediately before the start of each experiment.

^{19}F NMR spectroscopy

All ^{19}F NMR experiments were performed using a Varian VNMRS 500 MHz NMR spectrometer equipped with a double-tuned ^{1}H ^{19}F probe. 5 mm Shigemi NMR tubes (Shigemi Inc, BMS-005V) were used for this study. A series of ^{19}F spectra were recorded without spinning immediately after filtration of the sample as described above. For time course experiments, each ^{19}F spectrum was acquired from 512 transients with a 1.0 s pulse delay between each transient. To measure solvent isotope-induced changes in chemical shifts, samples were first prepared with 10% D_2O in PBS (pH 7.4) and spectra acquired as above. The samples were then diluted with D_2O to give a final mole fraction of 70% D_2O. ^{19}F chemical shifts were referenced to trifluoroethanol (TFE) at 0 ppm, and ^{19}F signal intensity was normalized to TFE. Line broadening of 2.0 Hz was used to process the final spectra. Origin 8.5 and Mestrenova was used for plotting the data.

The hydrodynamic radius of the initial conformation of the peptide was approximated by measuring the diffusion constant of the ^{19}F resonance by diffusion-ordered NMR experiments (DOSY). ^{19}F DOSY experiments were carried out using the gradient-

compensated stimulated echo (GCSTE) sequence with squared gradient pulses of constant duration (2 ms) and a variable gradient amplitude along the longitudinal axis.(32) Other experimental parameters include a 90° pulse width of 9.5 μs, a gradient stabilization delay of 0.5 ms, a stimulated-echo delay of 50 ms, a recycle delay of 0.5 s, and a spectral width of 25.51 kHz. Radio frequency pulses were phase cycled to remove unwanted echoes. 2048 transients were collected for each gradient and 10 gradients were collected for each sample for a total experimental time of approximately 6 hours. The stability of the sample was confirmed by comparison of the ^{19}F spectra at the beginning and end of the DOSY experiment. All spectra were processed with 3 Hz exponential line broadening prior to Fourier transformation. The diffusion coefficients were determined from the slope of a log plot of the intensity as a function of gradient strength using the Stejskal-Tanner equation. (33) The hydrodynamic radius was then calculated from the diffusion coefficient using the Einstein-Stokes relation and the viscosity of water at 25 °C.

Circular Dichroism (CD)

CD measurements were performed with an Aviv 62DS spectropolarimeter using a 0.1 cm pathlength cell. The samples were prepared similarly as for the NMR experiments. Molar CD per residue values were calculated using $\varepsilon = \theta_{obsd}/(3298 * l * c * n)$ where θ_{obsd} is the ellipticity measured in millidegrees, c is the molar concentration, l is the cell path length in centimeters, and n is the number of residues in the peptide.

Atomic Force Microscopy (AFM)

Aliquots were directly taken from samples prepared as described, and diluted 5-fold in buffer. Samples were spotted on SiO_2 substrates and imaged using a Nanoscope III microscope (Digital Instruments/Veeco Metrology Group).

Electrospray Ionization Mass Spectrometry (ESI-MS)

Protein ions were generated using a nESI source and optimized to allow transmission of noncovalent protein complexes. Nanoflow electrospray capillaries were prepared in-house as previously described.(34) To generate protein complex ions, an aliquot of the sample (*ca.* 5 μL) was sprayed from the nESI emitter using capillary voltages ranging from 1.4 kV, with the source operating in positive ion mode and the sample cone operated at 100 V. The mass spectra were acquired on a Synapt G2 (Waters, Milford MA) with the following settings and tuned to avoid ion activation and preserve non-covalent protein–ligand complexes. The bias voltage was 45 V, with backing pressure at 7.3 mBar and ToF pressure at 7.77×10^{-7} mBar. Mass spectra were calibrated externally using a solution of cesium iodide (100 mg/mL) and analyzed using Masslynx 4.1 and Driftscope 2.0 software (Waters). Samples were prepared by mixing an aliquot of the NMR sample with 100 mM ammonium acetate at pH 7.0 at 1:1 ratio followed by filtration through a 100 kDa Microcon filter (Millipore). Some samples were additionally filtered through a 30 kDa Microcon filter as described.

RESULTS

Design and Synthesis of $A\beta_{1-40}$-tfMet35

To study the process of Aβ aggregation using ^{19}F NMR, we synthesized a ^{19}F-labeled $A\beta_{1-40}$ peptide ($A\beta_{1-40}$-tfMet35) in which Met-35 was replaced by trifluoromethionine (tfMet) (Figure S1). Met-35 was chosen as a site at which a CF_3-group could readily be introduced in a minimally perturbing fashion. In addition, a fluorine nucleus on the flexible Met side-chain undergoes additional motional averaging that contributes to a smaller effective rotational correlation time, which, in turn, increases the probability of detecting larger aggregates. The ^{19}F chemical shifts and line-widths of the trifluoromethyl group

should change significantly if the peptide changes either its secondary structure or oligomerization state, as has been observed for other fluorinated peptides and proteins.(20) In particular, if oligomeric intermediates on the amyloid-forming pathway accumulate to an appreciable extent they should be detectable by NMR, provided they are not so large that their line-widths are broadened excessively, as is the case for amyloid fibers.(9)

To construct the $A\beta_{1\text{-}40}$-tfMet35 peptide, Fmoc-tfMet-Oh was first synthesized with the use of Togni reagent for trifluoromethylation as shown in Figure S1.(30) This optimized synthetic route improves yields by reducing the number of synthetic steps from 5 to 3 and eliminates the need for a chiral resolution. $A\beta_{1\text{-}40}$-tfMet35 was then synthesized from Fmoc-tfM-Oh using an optimized Fmoc procedure, as described under Experimental Procedures.

$A\beta_{1\text{-}40}$-tfMet35 reversibly forms oligomers immediately after preparation at high concentration

Recent studies have shown the pathway of $A\beta_{1\text{-}40}$ amyloid formation is strongly dependent on the initial concentration.(35, 36) To examine these differences, two samples of $A\beta_{1\text{-}40}$-tfMet35 were prepared at 4-fold different concentrations (46 μM and 182 μM) and their aggregation followed in parallel. The ^{19}F NMR spectra of both samples immediately after preparation are shown in Figure 1. Both spectra show a single intense resonance at 35.85 ppm (Figure 1A and B), which DOSY experiments show corresponds to a species with a hydrodynamic radius of 1.28 nm (Figure S2). This value is nearly identical to previous values obtained for non-aggregated $A\beta_{1\text{-}40}$ in buffer (1.29 nm) and in NaOH (1.32 nm)(37) and similar to single molecule measurements of monomeric $A\beta_{1\text{-}40}$ (0.9 nm).(38) The main resonance in the ^{19}F spectra at the initial time point is therefore very likely to correspond to the monomeric peptide in both samples.

However, differences between the two samples are apparent even at this initial time point. Rodlike short protofibers can be seen at the initial time-point in AFM images of the high concentration sample (Figure 1E), whereas they are absent in the low concentration sample (Figure 1D). Consistent with this finding, the high concentration sample shows a strong β-sheet component in the CD spectrum, as expected of protofibers. However this signal is absent in the low concentration sample (Figure 1C). The change in the CD spectra of the high concentration sample after ultrafiltration through 100 kDa cutoff membrane confirmed the β-sheet component arises from larger oligomers (Figure 1C). The presence of large oligomeric species at the initial time point can also be indirectly inferred from the ^{19}F spectra. The signal intensity of the 182 μM sample is 44% less than the 46 μM sample after normalization for concentration, consistent with the formation of large, NMR-invisible protofibers which give rise to the β-sheet CD spectra and observed in the AFM images (Figure 1E). Perhaps surprisingly in light of the large thermodynamic favorability of β-sheet formation in amyloid fibers,(38) oligomer formation of this type appears to be reversible. The CD spectrum after dilution from 182 μM to 46 μM reverts to a largely random coil conformation within the first scan without any filtration (Fig. 1C). The normalized intensity of the peak at 35.85 ppm also increases upon dilution (Fig. S3). Similarly, a small additional peak at 35.75 ppm observed at high (but not low) concentration disappears upon dilution (Figure S3).

Time course of $A\beta_{1\text{-}40}$-tfMet35 aggregation monitored by ^{19}F NMR, CD, and AFM

The time course of $A\beta_{1\text{-}40}$-tfMet35 oligomerization was followed by ^{19}F NMR and CD spectroscopy over a period of 1176 hours (7 weeks). The changes in the ^{19}F spectra of $A\beta_{1\text{-}40}$-tfMet35 observed over this time are shown in Figures 2 and 3; the corresponding changes in the CD spectra are shown in Figure 4. It is evident from the NMR spectra that various different species are formed and decay over this time period; for the high

concentration sample at least 5 species are evident after 840 hours (Figure 5A). Notably, Aβ oligomerization appears to follows a very different pathway from that of IAPP, for which no intermediates could be observed by NMR.(20) Figure 5 show the intensity of the various ^{19}F peaks plotted as a function of time for both samples, together with the corresponding changes in intensity of the CD signal.

It is evident that the monomeric peptide is depleted from the sample without a noticeable lag phase, although this occurs more slowly in the low concentration sample (Figures 5B and 5C). Fewer species were observed in the low concentration sample, which may reflect a concentration-dependent change in the aggregation pathway or that the poorer signal-to-noise ratio associated with the lower concentration prevented some oligomers from being observed. Even at after 7 weeks, a significant fraction of the sample remains as non-fibrillar oligomers as evidenced by sharp peaks in the NMR spectra. This suggests that these species may not be intermediates in the pathway to amyloid formation, but represent other non-fibrillar, oligomeric products of Aβ aggregation.

Of particular interest is a small peak at 35.83 ppm in the spectra that is initially present as a shoulder of the monomeric peak at 35.85 ppm. This resolves into a well-defined peak as the intensity of the monomer peak decreases (Figure 2), corresponding to either a low-molecular weight oligomer or a conformation of the monomer in slow exchange with a large, NMR-invisible oligomer.(35, 36, 39, 40) The intensity of this peak increases rapidly initially before reaching a maximum at 48 hours and decaying (Figure 5D). This time profile is characteristic of a kinetic intermediate and suggests at least one type of non-fibrillar oligomer is formed early during the lag phase for amyloid formation.

Analysis of the CD spectra of the low concentration sample shows a slow conversion of the peptide from the random coil conformation (minimum at 200 nm) to another species characterized by a minimum at 205 nm, followed by the later conversion of the peptide to a β-sheet conformation (minimum at 215 nm) (Figure 4A). The change from a minimum at 200 nm to 205 nm occurs on approximately the same time scale as the decrease in intensity of the ^{19}F NMR signal associated with monomeric Aβ (Figures 2 and 5C). However, the minimum at 205 nm does not correspond to the known CD spectrum of $A\beta_{1\text{-}40}$ amyloid fibers. (41) Instead, a minimum at 205 nm matches the CD spectra of several types of purified non-fibrillar oligomers of $A\beta_{1\text{-}40}$.(41)

Interpretation of the CD spectra for the high concentration sample was hindered by the fact the sample was too concentrated to obtain data at wavelengths lower than 206 nm. The CD spectrum at the initial time point (Figure 1C) exhibits a minimum at 215 nm characteristic of β-sheet structure. AFM images of the sample indicate that this is due to the presence of protofibers in the sample (Figure 1E). The protofibers could be removed by ultrafiltration, after which the CD spectrum of the filtrate indicated that the remaining peptide adopts a random coil conformation (Figure 1C). The protofibers are too large to be detected in the ^{19}F NMR experiment, so only the signal due to the monomeric peptide is observed at t = 0. The proportion of β-sheet structure (monitored by CD) in the sample increased over the first 72 hours of the experiment to reach a plateau (Figure 5B). The change in CD spectrum of the sample occurs more rapidly than the depletion of Aβ monomer, which is monitored by ^{19}F NMR. This suggests that further conversion of the NMR-invisible protofibers into a conformation with a larger fraction of β-sheet takes place during this initial time period.

Characterization of $A\beta_{1\text{-}40}$-tfMet35 aggregates formed at later times

After monomeric Aβ has nearly all been converted to other species (after ~ 600 h for both the high and low concentration samples), two new peaks begin to appear in the ^{19}F NMR spectra. For both the low and high concentration samples two new peaks are clearly visible

at 35.77 and 35.73 ppm. (Figures 2 and 3) In addition, two minor peaks near 35.65 and 35.57 ppm are visible in the high concentration sample. The AFM images taken after 24 hours (Fig. S4c) and 45 days (Fig. S4d) are similar, suggesting that the aggregates corresponding to the new peaks are significantly smaller than the protofibers visible in the AFM images.

To characterize these new oligomeric peaks, we attempted to estimate the molecular weight of $A\beta_{1\text{-}40}$-tfMet35 aggregates from filtration and electrospray ionization ion mobility mass spectrometry (ESI-IMMS) experiments.(24, 42) The M_r of the material corresponding to the new peaks was initially estimated by recording the ^{19}F NMR spectra of the low concentration sample after filtration through first a 100 kDa cutoff ultrafiltration membrane and then a 30 kDa cutoff membrane (Figure S5). The intensities of both peaks were reduced slightly by filtration through the 100 kDa cutoff membrane and more significantly by the 30 kDa cutoff membrane. For the 100 kDa membrane, the degree of attenuation was similar for both peaks. For the 30 kDa membrane, by contrast, the intensity of the 35.73 ppm was significantly more reduced than the 35.77 ppm peak. These findings indicate the oligomers corresponding to both peaks are between 100 kDa and 30 kDa in size, with the 35.77 ppm oligomer closer to 30 kDa than 100 kDa.

ESI-MS experiments showed similar results (Figure S6). The ESI-MS spectra for fresh, high-concentration samples show a single grouping of peaks corresponding to the protonated pseudomolecular ions for the +3 and +4 charge states of $A\beta_{1\text{-}40}$-tfMet35, along with sodium and other adducts related to the 20 mM phosphate buffer, consistent with primarily monomeric peptide. After incubation for 35 days (high concentration sample) or 52 days (low concentration sample) and ultrafiltration through a 100 kDa cutoff membrane, no peaks corresponding to monomeric Aβ peaks are evident and a broad set of peaks corresponding to unresolved, high molecular weight oligomers is observed instead. These peaks disappear after filtration through a 30 KDa cutoff membrane, consistent with the NMR results. These results therefore confirm both peaks likely correspond to aggregates between 30 and 100 kDa in size.

To gain insight into the secondary structure associated with these oligomeric species, at the end of the aggregation experiment we incubated the samples with Orange G. This dye is a derivative of Congo Red that specifically intercalates between stacked β-sheets.(43) Addition of 1 equivalent of Orange G to the high concentration sample resulted in an immediate decrease of the peak at 35.73 ppm and eventually, after 9 days, its complete disappearance from the spectrum. At the same time, the intensity of the peak at 35.77 ppm strongly increased (Figure. S7). Because Orange G binds to the interface between β-sheets, (43) the perturbation of the NMR spectra by this reagent suggests both peaks correspond to structures that contain a β-sheet binding site. The shift in intensity from 35.73 ppm to 35.77 ppm may be explained by the inter-conversion of the larger oligomer to the smaller by Orange G, possibly by intercalating between β-sheets in a manner similar to another amyloid binding compound, EGCG. (44)

Finally, we examined the solvent exposure of the Met35 side-chain by examining the influence of solvent isotope effect (H_2O/D_2O) on the ^{19}F chemical shift of $A\beta_{1\text{-}40}$-tfmMet35. Changing the solvent from 10 % D_2O to 70 % D_2O resulted in an upfield shift for both peaks of 0.06 ppm (Figure S8), which is similar to the shift for the trifluoroethanol internal standard (0.09 ppm). This observation indicates that the tfmMet35 side-chain is relatively solvent exposed in the oligomeric species that give rise to the NMR signal. Notably, this result is not consistent with current triangular models of $A\beta_{1\text{-}40}$ amyloid fibers, in which the C-terminus is sequestered within an internal cavity within the fiber.(45, 46)

However, it is consistent with several current models of smaller protofibers and non-fibrillar oligomers in which the Met35 side-chain is exposed.(47)

This behavior is quite different from that observed for IAPP-tfmPhe23 in which the kinetics of monomer consumption were sigmoidal; the intensity of the IAPP-tfmPhe23 monomer peak remained constant for a significant lag phase before dropping sharply.(20) The sigmoidal kinetics observed for monomer depletion by ^{19}F NMR reflected the kinetics of fiber formation, with close correspondence between the rate of monomer depletion measured by ^{19}F NMR and CD measurements of secondary structure and ThT measurements of fiber formation. (20) Similarly, time-lapse TEM images of fiber formation of IAPP-tfmPhe23 show only that the density of fibers increases as time progresses; non-fibrillar oligomers do not form a major population of IAPP-tfmPhe23 at any time.(20)

DISCUSSION

Several oligomeric, non-fibrillar structures of $A\beta_{1-40}$ and $A\beta_{1-42}$ are highly neurotoxic, and as such, have been heavily investigated as downstream or upstream agents of Alzheimer's disease.(25, 48) Whereas detailed structural studies of Aβ oligomers are beginning to emerge,(47, 49, 50) most structural and toxicity studies have, by necessity, required stable and relatively pure preparations of Aβ oligomers.(51) Because the aggregation of Aβ naturally tends to lead to a heterogeneous mixture of oligomers and fibers, either purification steps or specialized conditions, such as the addition of SDS, (52) low temperature,(53) or cross-linking,(41, 54) that are designed to trap specific oligomers are usually necessary for these studies. It is frequently difficult to observe the full pathway from monomeric peptide to oligomer species to the amyloid fiber form under these conditions. Purification also disturbs the equilibrium between Aβ species which can obscure the normal kinetic pathway. Therefore, while these non-fibrillar structures are commonly referred to as "intermediates", the actual relationship of almost all non-fibrillar structures along the aggregation pathway is still poorly defined.(55)

The kinetics of amyloid formation typically show a characteristic sigmoidal pattern; amyloid formation is slow or non-existent during an early lag phase before a period of rapid growth. The simplest model to explain this behavior is nucleation dependent polymerization, in which the lag-phase reflects the time for a critical concentration of energetically unfavorable nuclei to form. However, for a process as complex as amyloid formation many kinetic models are also consistent with an apparent lag phase.(56) By directly monitoring the rate of monomer depletion during aggregation through ^{19}F NMR along with other biophysical techniques, we are able to show that the early phase of fiber formation actually consists of several distinct steps (Figure 6). We note that while Figure 6 represents the simplest model in agreement with the data, many other models are also consistent and full determination of the pathway may require either isolation of each species or single-molecule tracking through the aggregation pathway.(57–59)

In the first step, the monomeric protein is almost entirely converted into a high molecular weight oligomer with a high β-sheet content and proto-fibrillar morphology that is not detectable by ^{19}F NMR (oligomer O1 in Figure 6). Dilution experiments suggest this conversion is at least partially reversible, at least in the early stages (Figures 1 and S3). This step occurs without a discernible lag-phaseunder our conditions, in agreement with previous measurements of monomer depletion during $A\beta_{1-40}$ aggregation.(10) This behavior is not consistent with a simple nucleation dependent polymerization model and suggests a more complex model involving an on- or off-pathway intermediate is necessary.

The formation of multiple peptide species was directly detected by the ^{19}F reporter introduced into Aβ. Only one oligomeric species observed by NMR (oligomer O2 at 35.83 ppm in Figure 6) possesses characteristics of a true intermediate in that it builds up and decays early in the time course of the experiment. After the disappearance of this oligomer and a substantial delay, several different types of other low-molecular weight oligomers begin to appear that apparently coexist with the proto-fibrillar species. At least two major types of oligomers with apparent molecular weights between 30 and 100 kDa in size can be identified at this later stage based on the ^{19}F NMR signal and ultrafiltration experiments. The first species to appear, oligomer O3 at 35.77 ppm in Figure 6, is smaller than the second, later, oligomer detected (oligomer O4 at 35.73 ppm in Figure 6), but both likely possess a partial β-sheet structure based on amyloid dye binding experiments and the final CD spectra. At least two more minor populations of oligomers in the second step of aggregation can also be detected in addition to these two major populations (oligomers O5 and O6 at 35.65 and 35.57 ppm in Figure 6). The various lines of experimental evidence point to the formation of a heterogeneous mixture of small oligomers of Aβ Xthat exist in pseudo-equilibrium with fibers and protofibers during early stages of aggregation.

Like any *in vitro* assay, care must be taken when extrapolating these results to the actual *in vivo* aggregation of $A\beta_{1\text{-}40}$ in the cell. First, the aggregation of $A\beta_{1\text{-}40}$ was studied in isolation without any of the cofactors normally present in cell, many of which have been shown to have substantial effects on $A\beta_{1\text{-}40}$ aggregation.(60) The ^{19}F NMR technique is easy to extend in principle to more complicated solutions such as cell culture media containing protein chaperones or other inhibitors. This is a significant advantage over ^{1}H NMR in which the signal from the protein cofactor will tend to obscure the $A\beta_{1\text{-}40}$ signal. Second, the concentrations used in these experiments are much higher than the circulating concentration of $A\beta_{1\text{-}40}$, which is in the nanomolar range.(61) Controversy exists if $A\beta_{1\text{-}40}$ aggregation occurs primarily intra- or extracellularly.(62) Spontaneous aggregation of $A\beta_{1\text{-}40}$ in vitro does not occur until the concentration of $A\beta_{1\text{-}40}$ reaches the micromolar range.(63, 64) Recent data suggests $A\beta_{1\text{-}40}$ must be internalized into multivesicular bodies before aggregation occurs.(65) In such a case, the local concentration of $A\beta_{1\text{-}40}$ within vesicular bodies can increase by over two orders of magnitude beyond the extracellular circulating concentration.(66) Thus while the ^{19}F NMR results may not reflect the concentration ranges expected for extracellular aggregation, the lower concentration (46 YM) used approaches the expected concentration range for intracellular aggregation. Finally, our results were obtained without agitation with a limited air/water interface. While this is also the case for *in vivo* aggregation, many *in vitro results* on $A\beta_{1\text{-}40}$ aggregation have been obtained with agitation, which greatly enhances aggregation (a timescale of hours instead of days) and may lead to changes in mechanism (67) and alternate structures.(68)

In conclusion, we have demonstrated ^{19}F NMR to be useful techniques to probe the formation of complex mixtures of oligomeric species by the amyloidogenic peptide $A\beta_{1\text{-}40}$. Both the initial, reversible formation of oligomers, and at least two species of irreversibly formed aggregates could be detected. By combining ^{19}F NMR with other spectroscopic techniques, information on the secondary structure and approximate molecular weights of some of these species could be obtained. These types of experimental measurements are difficult to perform by other techniques, and the additional level of detail obtained by measuring the rate of monomer depletion by NMR may prove fruitful for further characterization of intermediates involved in amyloid formation.

Supplementary Material

Refer to Web version on PubMed Central for supplementary material.

Acknowledgments

Funding: This work was supported by grants from the National Institutes of Health (GM GM084018 and GM095640 to A.R.) and the Department of Defense Multidisciplinary University Research Initiative (DoD 59743-CH-MUR to E.N.G.M.). M.T.S. acknowledges the support of NIH-funded training grant T32 CA140044

Abbreviations

Aβ	amyloid beta
tfMet	trifluoromethionine
NMR	nuclear magnetic resonance
kDa	kiloDalton
IAPP	islet amyloid polypeptide
Fmoc-hCys-Oh	Fmoc-L-homocysteine
Fmoc-Osu	Fmoc *N*-hydroxysuccinimide ester
DMF	Dimethylformamide
TCEP	tris(2-carboxyethyl)phosphine
Fmoc-tfMet-Oh	Fmoc-L-trifluoromethionine
Togni reagent	1-Trifluoromethyl-3,3-dimethyl-1,2-benziodoxole
Dmb	dimethoxybenzyl
TFE	trifluoroethanol
PBS	phosphate buffered saline
DOSY	diffusion ordered spectroscopy
GCSTE	gradient-compensated stimulated echo
CD	circular dichroism
AFM	atomic force microscopy
ESI-MS	electrospray ionization mass spectrometry
ToF	time of flight
tfmPhe	triflouromethyl phenylalanine
TEM	transmission electron microscopy
EGCG	epigallocatechin gallate
SDS	sodium dodecyl sulfate

References

1. Harrison RS, Sharpe PC, Singh Y, Fairlie DP. Amyloid peptides and proteins in review. Rev Physiol Bioch P. 2007; 159:1–77.
2. Fandrich M. On the structural definition of amyloid fibrils and other polypeptide aggregates. Cell Mol Life Sci. 2007; 64:2066–2078. [PubMed: 17530168]
3. Jahn TR, Makin OS, Morris KL, Marshall KE, Tian P, Sikorski P, Serpell LC. The common architecture of cross-β amyloid. J Mol Biol. 2010; 395:717–727. [PubMed: 19781557]
4. Hamley IW. The amyloid beta peptide: a chemist's perspective. Role in Alzheimer's and fibrillization. Chem Rev. 112:5147–5192. [PubMed: 22813427]

5. Hardy JA, Higgins GA. Alzheimer's Disease - the amyloid cascade hypothesis. Science. 1992; 256:184–185. [PubMed: 1566067]
6. Hardy J. The amyloid hypothesis for Alzheimer's disease: a critical reappraisal. J Neurochem. 2009; 110:1129–1134. [PubMed: 19457065]
7. Hardy J, Selkoe DJ. The amyloid hypothesis of Alzheimer's disease: Progress and problems on the road to therapeutics. Science. 2002; 297:353–356. [PubMed: 12130773]
8. Pryor NE, Moss MA, Hestekin CN. Unraveling the early events of amyloid-beta protein (Aβ) aggregation: Techniques for the determination of Aβ aggregate size. Int J Mol Sci. 2012; 13:3038–3072. [PubMed: 22489141]
9. Mishra R, Geyer M, Winter R. NMR spectroscopic investigation of early events in IAPP amyloid fibril formation. ChemBioChem. 2009; 10:1769–1772. [PubMed: 19575373]
10. Yan YL, Wang CY. Aβ42 is more rigid than Aβ40 at the C-terminus: Implications for Aβ aggregation and toxicity. J Mol Biol. 2006; 364:853–862. [PubMed: 17046788]
11. Kitevski-LeBlanc JL, Prosser RS. Current applications of F-19 NMR to studies of protein structure and dynamics. Prog Nucl Mag Res Sp. 2012; 62:1–33.
12. Li H, Frieden C. Comparison of C40/82A and P27A C40/82A barstar mutants using F-19 NMR. Biochemistry. 2007; 46:4337–4347. [PubMed: 17371049]
13. Li HL, Frieden C. Observation of sequential steps in the folding of intestinal fatty acid binding protein using a slow folding mutant and F-19 NMR. Proc Natl Acad Sci U S A. 2007; 104:11993–11998. [PubMed: 17615232]
14. Li H, Frieden C. Fluorine-19 NMR studies on the acid state of the intestinal fatty acid binding protein. Biochemistry. 2006; 45:6272–6278. [PubMed: 16700539]
15. Li H, Frieden C. NMR studies of 4-F-19-phenylalanine-labeled intestinal fatty acid binding protein: Evidence for conformational heterogeneity in the native state. Biochemistry. 2005; 44:2369–2377. [PubMed: 15709749]
16. Wang GF, Li CG, Pielak GJ. Probing the micelle-bound aggregation-prone state of a-synuclein with ^{19}F NMR spectroscopy. Chembiochem ChemBioChem. 2010; 11:1993–1996.
17. Wang GF, Li CG, Pielak GJ. ^{19}F NMR studies of a-synuclein-membrane interactions. Prot Sci. 2010; 19:1686–1691.
18. Cobb SL, Murphy CD. ^{19}F NMR applications in chemical biology. J Fluorine Chem. 2009; 130:132–143.
19. Li CG, Wang GF, Wang YQ, Creager-Allen R, Lutz EA, Scronce H, Slade KM, Ruf RAS, Mehl RA, Pielak GJ. Protein ^{19}F NMR in Escherichia coli. J Am Chem Soc. 2010; 132:321–327. [PubMed: 20050707]
20. Suzuki Y, Brender JR, Hartman K, Ramamoorthy A, Marsh ENG. Alternative pathways of human islet amyloid polypeptide aggregation distinguished by ^{19}F nuclear magnetic resonance-detected kinetics of monomer consumption. Biochemistry. 2012; 51:8154–8162. [PubMed: 22998665]
21. Soong R, Brender JR, Macdonald PM, Ramamoorthy A. Association of highly compact type II diabetes related islet amyloid polypeptide intermediate species at physiological temperature revealed by diffusion NMR spectroscopy. J Am Chem Soc. 2009; 131:7079–7085. [PubMed: 19405534]
22. Vaiana SM, Ghirlando R, Yau WM, Eaton WA, Hofrichter J. Sedimentation studies on human amylin fail to detect low-molecular-weight oligomers. Biophys J. 2008; 94:L45–L47. [PubMed: 18223003]
23. Marek P, Mukherjee S, Zanni MT, Raleigh DP. Residue-specific, real-time characterization of lag-phase species and fibril growth during amyloid formation: A combined fluorescence and IR Study of p-cyanophenylalanine analogs of islet amyloid polypeptide. J Mol Biol. 2010; 400:878–888. [PubMed: 20630475]
24. Lee J, Culyba EK, Powers ET, Kelly JW. Amyloid-β forms fibrils by nucleated conformational conversion of oligomers. Nat Chem Biol. 2011; 7:602–609. [PubMed: 21804535]
25. Benilova I, Karran E, De Strooper B. The toxic Aβ oligomer and Alzheimer's disease: an emperor in need of clothes. Nat Neurosci. 2012; 15:349–357. [PubMed: 22286176]

26. Miller Y, Ma B, Nussinov R. Polymorphism in Alzheimer Aβ Amyloid organization reflects conformational selection in a rugged energy landscape. Chem Rev. 2010; 110:4820–4838. [PubMed: 20402519]
27. Ma BY, Nussinov R. Selective molecular recognition in amyloid growth and transmission and cross-species barriers. J Mol Biol. 2012; 421:172–184. [PubMed: 22119878]
28. Jiang L, Burgess K. Fluorinated and iodinated templates for syntheses of β-turn peptidomimetics. Tetrahedron. 2002; 58:8743–8750.
29. Duewel H, Daub E, Robinson V, Honek JF. Incorporation of trifluoromethionine into a phage lysozyme: Implications and a new marker for use in protein ^{19}F NMR. Biochemistry. 1997; 36:3404–3416. [PubMed: 9116020]
30. Kieltsch I, Eisenberger P, Togni A. Mild electrophilic trifluoromethylation of carbon- and sulfur-centered nucleophiles by a hypervalent iodine(III)-CF3 reagent. Angew Chem Int Edit. 2007; 46:754–757.
31. Garner DK, Vaughan MD, Hwang HJ, Savelieff MG, Berry SM, Honek JF, Lu Y. Reduction potential tuning of the blue copper center in Pseudomonas aeruginosa azurin by the axial methionine as probed by unnatural amino acids. J Am Chem Soc. 2006; 128:15608–15617. [PubMed: 17147368]
32. Pelta MD, Barjat H, Morris GA, Davis AL, Hammond SJ. Pulse sequences for high-resolution diffusion-ordered spectroscopy (HR-DOSY). Magn Reson Chem. 1998; 36:706–714.
33. Stejskal EO, Tanner JE. Spin diffusion measurements: Spin Echoes in the presence of a time-dependent field gradient. J Chem Phys. 1965; 42:288–292.
34. Hernández H, Robinson CV. Determining the stoichiometry and interactions of macromolecular assemblies from mass spectrometry. Nat Prot. 2007; 2:715–726.
35. Fawzi NL, Ying J, Torchia DA, Clore GM. Kinetics of amyloid β monomer-to-oligomer exchange by NMR relaxation. J Am Chem Soc. 2010; 132:9948–9951. [PubMed: 20604554]
36. Fawzi NL, Ying JF, Ghirlando R, Torchia DA, Clore GM. Atomic-resolution dynamics on the surface of amyloid-β protofibrils probed by solution NMR. Nature. 2011; 480:268–272. [PubMed: 22037310]
37. Pedersen MO, Mikkelsen K, Behrens MA, Pedersen JS, Enghild JJ, Skrydstrup T, Malmendal A, Nielsen NC. NMR reveals two-step association of Congo Red to amyloid β in low-molecular-weight aggregates. J Phys Chem B. 2010; 114:16003–16010. [PubMed: 21077638]
38. Nag S, Sarkar B, Bandyopadhyay A, Sahoo B, Sreenivasan VKA, Kombrabail M, Muralidharan C, Maiti S. Nature of the amyloid-β monomer and the monomer-oligomer equilibrium. J Biol Chem. 2011; 286:13827–13833. [PubMed: 21349839]
39. Krishnamoorthy J, Brender JR, Vivekanandan S, Jahr N, Ramamoorthy A. Side-chain dynamics reveals transient association of Aβ(1-40) monomers with amyloid fibers. J Phys Chem B. 2012; 116:13618–13623. [PubMed: 23116141]
40. Narayanan S, Reif B. Characterization of chemical exchange between soluble and aggregated states of β-amyloid by solution-state NMR upon variation of salt conditions. Biochemistry. 2005; 44:1444–1452. [PubMed: 15683229]
41. Ono K, Condron MM, Teplow DB. Structure-neurotoxicity relationships of amyloid beta-protein oligomers. Proc Natl Acad Sci U S A. 2009; 106:14745–14750. [PubMed: 19706468]
42. Bernstein SL, Dupuis NF, Lazo ND, Wyttenbach T, Condron MM, Bitan G, Teplow DB, Shea JE, Ruotolo BT, Robinson CV, Bowers MT. Amyloid-β protein oligomerization and the importance of tetramers and dodecamers in the aetiology of Alzheimer's disease. Nat Chem. 2009; 1:326–331. [PubMed: 20703363]
43. Landau M, Sawaya MR, Faull KF, Laganowsky A, Jiang L, Sievers SA, Liu J, Barrio JR, Eisenberg D. Towards a Pharmacophore for Amyloid. PLoS Biol. 2011; 9:e1001080. [PubMed: 21695112]
44. del Amo JML, Fink U, Dasari M, Grelle G, Wanker EE, Bieschke J, Reif B. Structural properties of EGCG-induced, nontoxic Alzheimer's disease Aβ oligomers. J Mol Biol. 2012; 421:517–524. [PubMed: 22300765]

45. Paravastu AK, Leapman RD, Yau WM, Tycko R. Molecular structural basis for polymorphism in Alzheimer's β-amyloid fibrils. Proc Natl Acad Sci U S A. 2008; 105:18349–18354. [PubMed: 19015532]
46. Tycko R. Solid-State NMR Studies of Amyloid Fibril Structure. Ann Rev Phys Chem. 2011; 62:279–299. [PubMed: 21219138]
47. Stroud JC, Liu C, Teng PK, Eisenberg D. Toxic fibrillar oligomers of amyloid-β have cross-β structure. Proc Natl Acad Sci U S A. 2012; 109:7717–7722. [PubMed: 22547798]
48. Fandrich M. Oligomeric intermediates in amyloid formation: Structure determination and mechanisms of toxicity. J Mol Biol. 421:427–440. [PubMed: 22248587]
49. Scheidt HA, Morgado I, Huster D. Solid-state NMR reveals a close structural relationship between amyloid-β protofibrils and oligomers. J Biol Chem. 2012; 287:22822–22826. [PubMed: 22589542]
50. Chimon S, Shaibat MA, Jones CR, Calero DC, Aizezi B, Ishii Y. Evidence of fibril-like β-sheet structures in a neurotoxic amyloid intermediate of Alzheimer's β-amyloid. Nat Struct Mol Biol. 2007; 14:1157–1164. [PubMed: 18059284]
51. Rosensweig C, Ono K, Murakami K, Lowenstein DK, Bitan G, Teplow DB. Preparation of Stable Amyloid beta-Protein Oligomers of Defined Assembly Order. Methods Mol Biol. 2012; 849:23–31. [PubMed: 22528081]
52. Yu LP, Edalji R, Harlan JE, Holzman TF, Lopez AP, Labkovsky B, Hillen H, Barghorn S, Ebert U, Richardson PL, Miesbauer L, Solomon L, Bartley D, Walter K, Johnson RW, Hajduk PJ, Olejniczak ET. Structural characterization of a soluble amyloid β-peptide oligomer. Biochemistry. 2009; 48:1870–1877. [PubMed: 19216516]
53. Lambert MP, Barlow AK, Chromy BA, Edwards C, Freed R, Liosatos M, Morgan TE, Rozovsky I, Trommer B, Viola KL, Wals P, Zhang C, Finch CE, Krafft GA, Klein WL. Diffusible, nonfibrillar ligands derived from Aβ(1-42) are potent central nervous system neurotoxins. Proc Natl Acad Sci U S A. 1998; 95:6448–6453. [PubMed: 9600986]
54. Yamaguchi T, Yagi H, Goto Y, Matsuzaki K, Hoshino M. A Disulfide-Linked Amyloid-β peptide dimer forms a protofibril-like oligomer through a distinct pathway from amyloid fibril formation. Biochemistry. 49:7100–7107. [PubMed: 20666485]
55. Cohen SIA, Vendruscolo M, Dobson CM, Knowles TPJ. From macroscopic measurements to microscopic mechanisms of protein aggregation. J Mol Biol. 2012; 421:160–171. [PubMed: 22406275]
56. Morris AM, Watzky MA, Finke RG. Protein aggregation kinetics, mechanism, and curve-fitting: A review of the literature. Biochim Biophys Acta. 2009; 1794:375–397. [PubMed: 19071235]
57. Liang Y, Lynn DG, Berland KM. Direct observation of nucleation and growth in amyloid self-assembly. J Am Chem Soc. 2010; 132:6306–6308. [PubMed: 20397724]
58. Ban T, Yamaguchi K, Goto Y. Direct observation of amyloid fibril growth, propagation, and adaptation. Acc Chem Res. 2006; 39:663–670. [PubMed: 16981683]
59. Knowles TPJ, White DA, Abate AR, Agresti JJ, Cohen SIA, Sperling RA, De Genst EJ, Dobson CM, Weitz DA. Observation of spatial propagation of amyloid assembly from single nuclei. Proc Natl Acad Sci U S A. 2011; 108:14746–14751. [PubMed: 21876182]
60. Alexandrescu AT. Amyloid accomplices and enforcers. Protein Sci. 2005; 14:1–12. [PubMed: 15576561]
61. Kuo YM, Emmerling MR, Lampert HC, Hempelman SR, Kokjohn TA, Woods AS, Cotter RJ, Roher AE. High levels of circulating Aβ42 are sequestered by plasma proteins in Alzheimer's disease. Biochem Biophys Res Commun. 1999; 257:787–791. [PubMed: 10208861]
62. Hoozemans JJM, Chafekar SM, Baas F, Eikelenboom P, Scheper W. Always around, never the same: Pathways of amyloid β induced neurodegeneration throughout the pathogenic cascade of Alzheimer's disease. Curr Med Chem. 2006; 13:2599–2605. [PubMed: 17017913]
63. O'Nuallain B, Shivaprasad S, Kheterpal I, Wetzel R. Thermodynamics of Aβ(1-40) amyloid fibril elongation. Biochemistry. 2005; 44:12709–12718. [PubMed: 16171385]
64. Huang THJ, Yang DS, Fraser PE, Chakrabartty A. Alternate aggregation pathways of the Alzheimer β-amyloid peptide - An in vitro model of preamyloid. J Biol Chem. 2000; 275:36436–36440. [PubMed: 10961999]

65. Friedrich RP, Tepper K, Roznicke R, Soom M, Westermann M, Reymann K, Kaether C, Fandrich M. Mechanism of amyloid plaque formation suggests an intracellular basis of Aβ pathogenicity. Proc Natl Acad Sci U S A. 2010; 107:1942–1947. [PubMed: 20133839]

66. Hu XY, Crick SL, Bu GJ, Frieden C, Pappu RV, Lee JM. Amyloid seeds formed by cellular uptake, concentration, and aggregation of the amyloid-β peptide. Proc Natl Acad Sci U S A. 2009; 106:20324–20329. [PubMed: 19910533]

67. Pronchik J, He XL, Giurleo JT, Talaga DS. In vitro formation of amyloid from a-synuclein is dominated by reactions at hydrophobic interfaces. J Am Chem Soc. 2010; 132:9797–9803. [PubMed: 20578692]

68. Petkova AT, Leapman RD, Guo ZH, Yau WM, Mattson MP, Tycko R. Self-propagating, molecular-level polymorphism in Alzheimer's β-amyloid fibrils. Science. 2005; 307:262–265. [PubMed: 15653506]

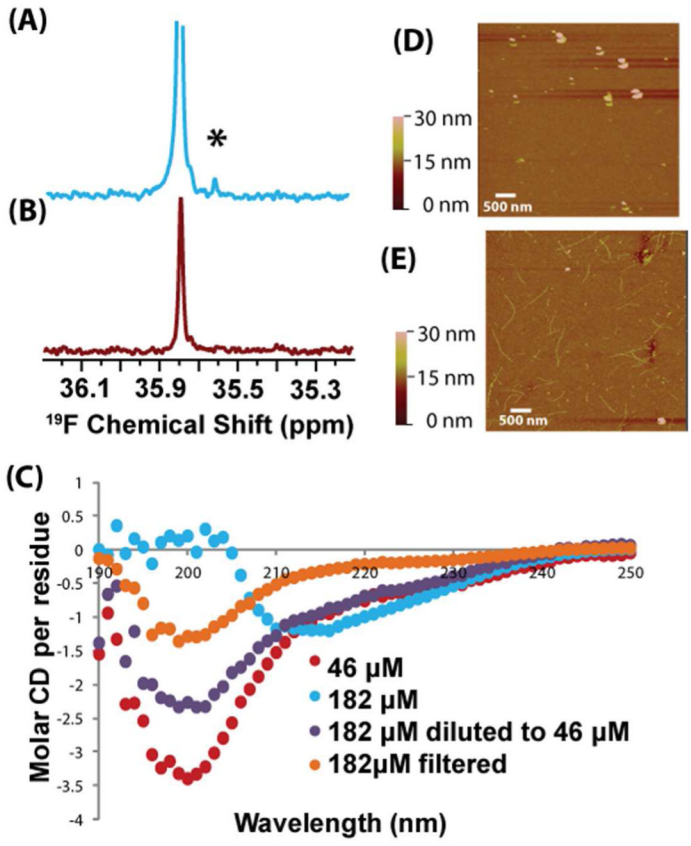

Figure 1.

Characterization of $A\beta_{1\text{-}40}$-tfM_{35} immediately after preparation. **(A)** and **(B)**: ^{19}F NMR spectra of, respectively, 182 μM and 46 μM samples of $A\beta_{1\text{-}40}$-tfM_{35}; a small additional peak not present in the low concentration sample is marked with an asterisk. The intensity of both samples is normalized to an internal TFE standard. **(C)**: CD spectra of 182 μM and 46 μM samples of $A\beta_{1\text{-}40}$-tfM_{35} taken at the initial time-point and the change in spectrum after filtration of the 182 μM sample. **(D)** and **(E)**: AFM images of, respectively, 46 μM and 182 μM samples of $A\beta_{1\text{-}40}$-tfM_{35} on SiO_2 substrates taken at the initial time-point.

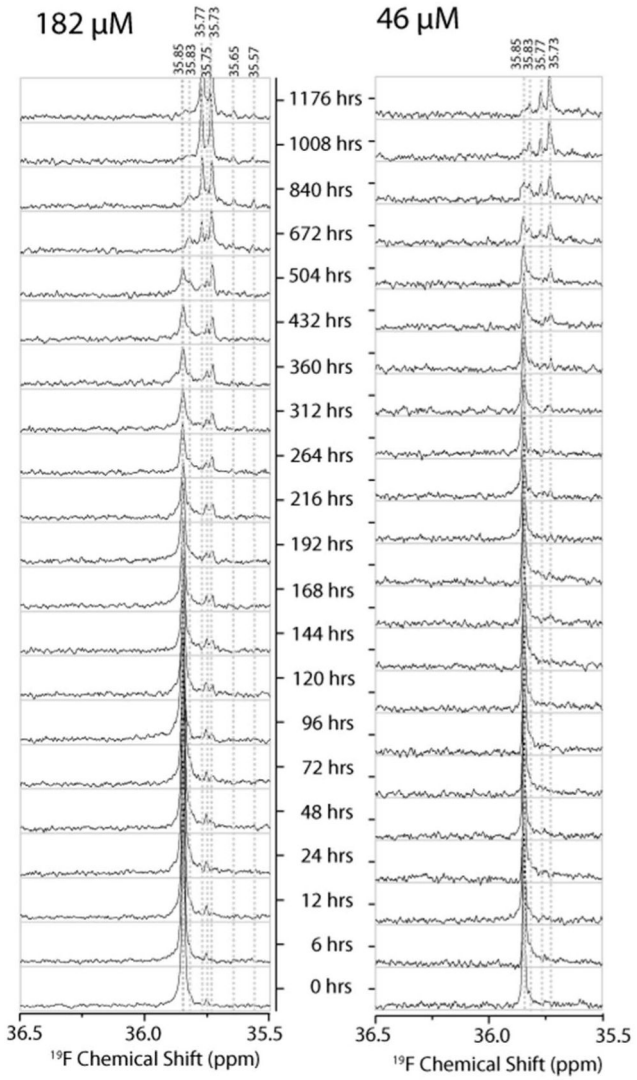

Figure 2.

Time course of $A\beta_{1\text{-}40}$-tfM_{35} aggregation followed by ^{19}F NMR. *Left:* sample concentration = 182 μM; *Right*: sample concentration = 46 μM. Sample spectra were measured in parallel; the signal intensity of each spectrum was normalized to an internal TFE standard.

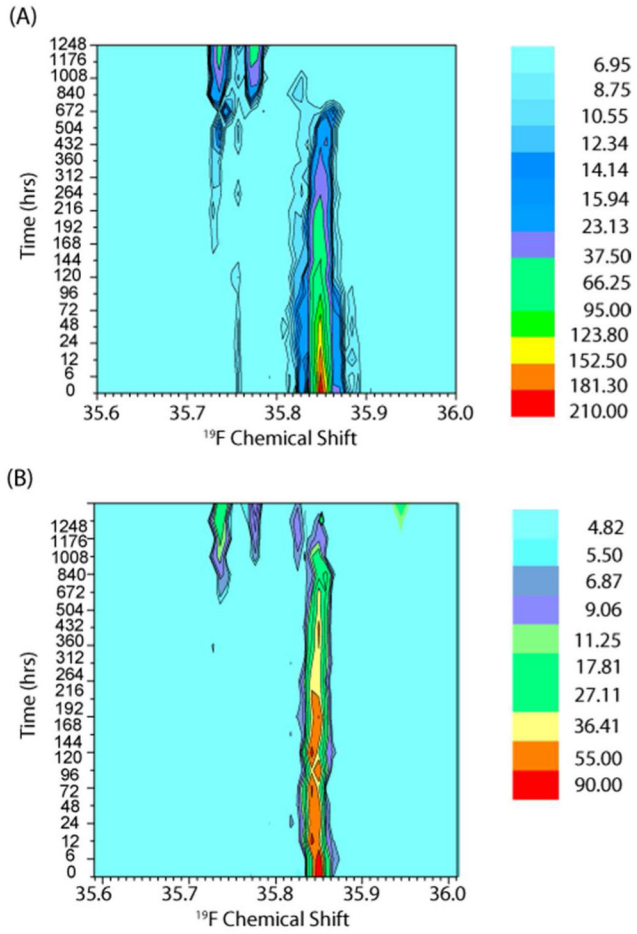

Figure 3.

Contour plots showing changes in the ^{19}F spectrum of $A\beta_{1\text{-}40}$-tfM_{35} as a function of time (vertical axis). (A) $A\beta_{1\text{-}40}$-tfM_{35} concentration = 182 μM; (B) $A\beta_{1\text{-}40}$-tfM_{35} concentration = 46 μM.

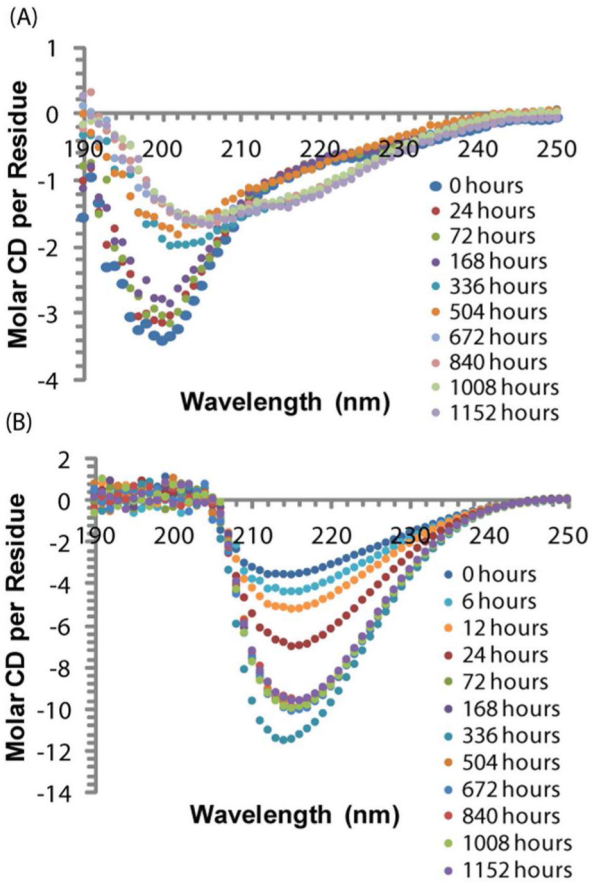

Figure 4.

Changes to the secondary structure of $A\beta_{1\text{-}40}$-tfM_{35} followed by CD spectroscopy. **(A)** Sample concentration = 46 μM; **(B)** Sample concentration = 182μM.

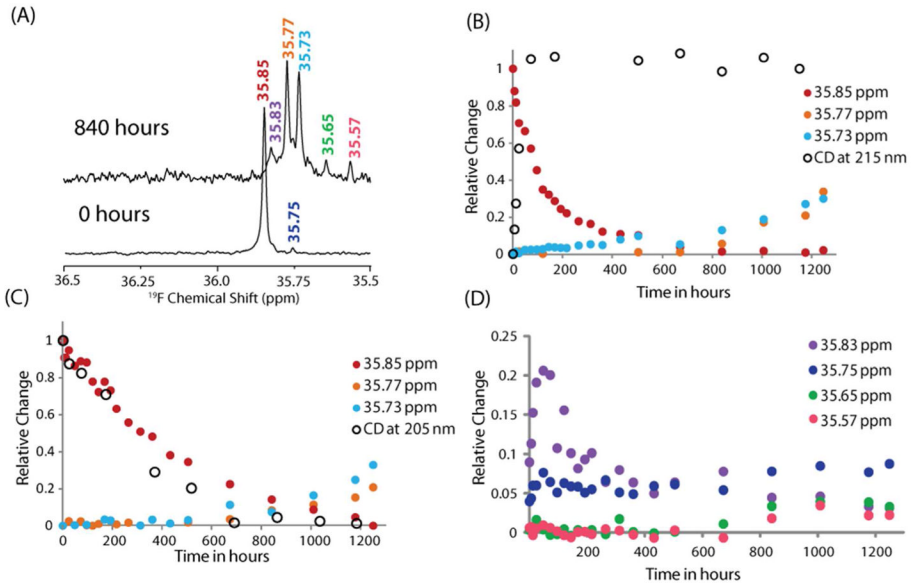

Figure 5.

Kinetics of aggregation followed by ^{19}F NMR and CD spectroscopy. **(A)**: Representative spectrum of a 182 μM sample of $A\beta_{1\text{-}40}$-tfM_{35} indicating the major and minor peaks. **(B)**: Kinetics of aggregation of followed by plotting peak intensity as a function of time for the major peaks in the ^{19}F NMR spectrum of the 182 μM sample of $A\beta_{1\text{-}40}$-tfM_{35}. The changes in the minimum at 215 nm in the CD spectrum are also plotted. (C): Data plotted as described in **(B)** for the 46 μM sample of $A\beta_{1\text{-}40}$-tfM_{35}, except that the CD changes are monitored at 205 nm. **(D)**: Time course for the formation and decay species represented by minor peaks in the ^{19}F NMR spectrum of the 182 μM sample. ^{19}F NMR values are normalized to the initial intensity of the monomer peak at 35.85 ppm. CD values are normalized to the initial and final values.

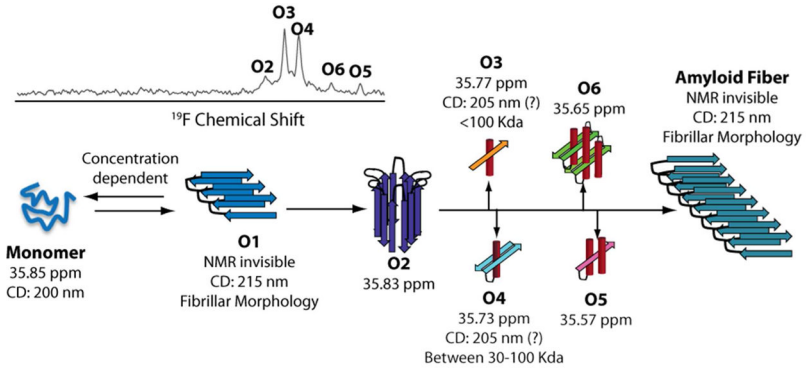

Figure 6.

A scheme describing a possible aggregation pathway for $A\beta_{1\text{-}40}$-tfM_{35} based on the different experimental data described above. The peaks corresponding to the various intermediates are marked on the ^{19}F spectrum.